HomoFRET Fluorescence Anisotropy Imaging as a Tool to Study Molecular Self-Assembly in Live Cells

Fiona T. S. Chan,[a] Clemens F. Kaminski,*[a, b] and Gabriele S. Kaminski Schierle[a]

Molecular self-assembly is a defining feature of numerous biological functions and dysfunctions, ranging from basic cell signalling to diseases mediated by protein aggregation. There is current demand for novel experimental methods to study molecular self-assembly in live cells, and thereby in its physiological context. Förster resonance energy transfer (FRET) between fluorophores of a single type, known as homoFRET, permits noninvasive detection and quantification of molecular clusters in live cells. It can thus provide powerful insights into the molecular physiology of living systems and disease. HomoFRET is detected by measuring the loss of fluorescence anisotropy upon excitation with polarised light. This article reviews recent key developments in homoFRET fluorescence anisotropy imaging for the detection and quantification of molecular self-assembly reactions in biological systems. A summary is given of the current state-of-the-art and case studies are presented of successful implementations, highlighting technical aspects which have to be mastered to bridge the gap between proof-of-concept experiments and biological discoveries.

1. Introduction

Many important biological functions, and dysfunctions, involve the self-assembly of molecules. Two well-characterised examples are the clustering of signalling proteins in cellular membranes (known as membrane rafts)[1] and the aggregation of proteins leading to neurodegenerative diseases.[2,3] A range of biophysical techniques, such as gel electrophoresis, NMR, electron microscopy, X-ray crystallography and optical spectroscopy[4–6] are available to inform one on the structure and size of the resulting molecular assemblies. However, traditional biophysical methods require extensive sample preparation, and hence are destructive in nature, constricting experiments to an in vitro or ex vivo context. Modern microscopic imaging techniques are, on the other hand, compatible with the study of live cells and organisms,[7–9] made possible by recent advances in molecular labelling techniques.[10–13] As a result, advanced molecular imaging techniques have led to a paradigm shift in the life sciences.

Theodor Förster's seminal work on the theory of resonance energy transfer has played an inestimable role in accelerating this revolution. Prompted by reflections on the efficiency of nature's light-harvesting process, namely photosynthesis, Förster developed already in 1946 a quantitative theory for the non-radiative transfer of excitation energy between fluorophores. This acts via a dipole–dipole electrostatic interaction in the 1–10 nm range, a length scale characteristic of biological molecules. Little was he to guess during his lifetime what the implications of his discoveries would be for modern biology.[14] Förster resonance energy transfer (FRET) is today used in laboratories all over the world to inform on phenomena that occur on the molecular scale. FRET is compatible with a range of microscopy techniques, improving on the resolution limit dictated by diffraction (typically 250 nm for visible light) by close to two orders of magnitude, opening our eyes to the molecular physiology of living systems and diseases.

FRET is now a staple method in biology for probing molecular interactions, conformations and subcellular organisation.[15] However, in the particular context of imaging the self-assembly of biological molecules in live cells, applications are only just emerging. A useful variant of FRET for this purpose is homoFRET, referring to the energy exchange between like fluorophores. HomoFRET, in contrast to heteroFRET, requires only a single fluorophore moiety for labelling and is detectable by measuring the loss of anisotropy (i.e. loss of polarisation) in the emission upon excitation with polarised light. Measurements of homoFRET by fluorescence anisotropy imaging microscopy (FAIM) have great potential for measuring molecular self-assembly in cells. It is thus timely to review the current state-of-the-art and to identify key barriers that need to be overcome for future breakthroughs. This article aims to provide an outlook on recent developments of homoFRET anisotropy imaging for molecular self-assembly, and focuses on aspects of its practical implementation that are vital to the successful transition from proof-of-concept experiments to new biological discoveries.

The structure of the article is as follows. The theory of FRET, and homoFRET in particular, is briefly described (readers

[a] F. T. S. Chan, Dr. C. F. Kaminski, Dr. G. S. Kaminski Schierle
Department of Chemical Engineering and Biotechnology
University of Cambridge
Pembroke Street, Cambridge, CB2 3RA (U.K.)
Fax: (+44) 1223-334-796
E-mail: cfk23@cam.ac.uk

[b] Dr. C. F. Kaminski
Friedrich-Alexander University of Erlangen-Nürnberg
D-91052, Erlangen (Germany)

should refer to refs. [16, 17] for more details). The instrumentation and calibration methods which have been developed for rigorous FAIM imaging in the microscope setting are then reviewed. Case studies of successful implementations to biological problem-solving are then discussed. Finally, key challenges and future promises are outlined.

2. Theoretical Background

2.1. Photophysics of FRET

An expression for the rate of FRET from a donor to an acceptor was first derived by Theodor Förster in 1946 based on a semi-classical theory.[18] His theory improved on a classical but incomplete model developed earlier by Perrin,[19] who first hypothesised on the existence of the long range dipole–dipole energy transfer [Eqs. (1) and (2)]:

$$k_{ET} = \frac{1}{\tau_D}\left(\frac{R_0}{R}\right)^6 \qquad (1)$$

$$R_0^6 \propto \frac{\kappa^2 \phi_D}{n^4}\Gamma \qquad (2)$$

The rate of FRET k_{ET} may be described by Equations (1) and (2), where τ_D is the radiative lifetime of the donor in the absence of FRET, R_0 is the Förster distance for a particular donor–acceptor pair, R is the donor–acceptor distance, κ is the dipole–dipole orientation factor, ϕ_D is the quantum yield of the donor, n is the refractive index of the medium, and Γ is the overlap integral between the donor emission and acceptor absorption spectra. R_0 for typical fluorophores is in the 2–5 nm range, and denotes the distance where the energy transfer efficiency from donor to acceptor reaches 50 %.

An important realisation by Förster was that a resonance condition between donor and acceptor dipoles must be fulfilled for FRET to occur, which is the case when the donor emission and the acceptor excitation spectra overlap. This gives rise to the integral term Γ in Equation (2). In heteroFRET, donor and acceptor fluorophores are spectrally distinct, and there is a choice of optimal fluorophores to maximise the overlap integral. HeteroFRET can be measured in fluorescence microscopy by measuring donor and acceptor emission intensity ratios, changes in the donor emission lifetime, intensity changes upon donor or acceptor photobleaching, and changes in emission anisotropy, all of which have been reviewed in ref. [20]. It should be noted, however, that complications in interpreting FRET signals may result from non-specific interactions or instrumental artefacts. Careful experimental design and controls are thus needed to avoid the common pitfalls in FRET experiments (summarised in refs. [21, 22]).

For homoFRET, only a single type of fluorophore is used and one with a small Stokes shift (i.e. an appreciable overlap between the emission and absorption spectra) is required. Since in this case the donors and acceptors are spectroscopically indistinguishable, intensity ratios or lifetime measurements cannot be used to quantify homoFRET. Measuring the fluorescence anisotropy, although just one of many ways to quantify heteroFRET, is the only established method of detecting homoFRET. HomoFRET between fluorophores whose dipole orientations are random has been shown to effectively randomise the polarisation of the acceptor-emitted fluorescence. Fluorescence anisotropy imaging microscopy (FAIM) is therefore a suitable method to detect homoFRET arising from molecular self-assembly in biology.

2.2. Probing Molecular Self-Assembly with HomoFRET

The phenomenon that FRET among molecules randomly oriented in close proximity (i.e. within R_0) results in randomisation of the fluorescence polarisation has been exploited to gain information on molecular self-assembly. Table 1 gives a summary of such biological studies with FAIM (case studies are discussed in detail in Section 4). While FAIM is applicable to both homo- and heteroFRET, homoFRET is preferred to heteroFRET for studies of self-assembly, as the requirement for only a single type of fluorescent label for the monomeric building blocks greatly simplifies the experimental procedure.

The concept of FAIM is to measure the polarisation orientation of the fluorescence relative to that of the excitation light in every image pixel. The fluorescence anisotropy r is conventionally defined as Equation (3):

$$r = \frac{I_{\parallel} - GI_{\perp}}{I_{\parallel} + 2GI_{\perp}} \qquad (3)$$

Table 1. Examples of homoFRET fluorescence anisotropy imaging of molecular self-assembly in biology.

| Self-assembly | | HomoFRET imaging | | |
Molecule	Function	Probe	Function	Ref.
GPI-anchored[a] folate receptor	Membrane clustering	PLF[e]	Detecting clusters	[30]
GPI[a]	Membrane clustering	GFP, mYFP	Detecting clusters and size distribution	[46]
GPI[a]	Membrane clustering	GFP	Cluster sizing	[33, 53]
HSV-1 TK[b]	Cell signalling	GFP	Detecting homo-dimers	[35]
erbB1[c]	Cell signalling	eGFP	Detecting homo-dimers	[50]
hM1[d]	Cell signalling	eGFP	Detecting homo-dimers	[52]
α-synuclein	Pathogenic protein aggregation	YFP	Detecting aggregates	[27]

[a] GPI = Glycosylphosphatidylinisotol, [b] HSV-1 TK = Herpes simplex virus thymidine kinase, [c] erbB1 = Epidermal growth factor receptor, [d] hM₁ = Human M1 muscarinic acetylcholine receptor subtype, [e] PLF = N$^\alpha$-pteroyl-N$^\varepsilon$-(4′-fluoresceinthiocarbamoyl)-L-lysine.
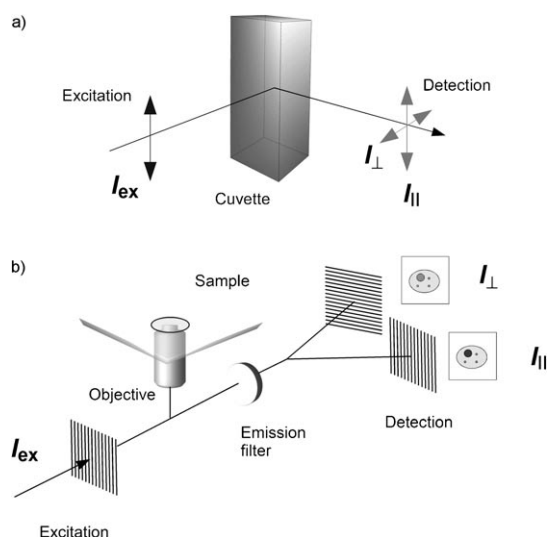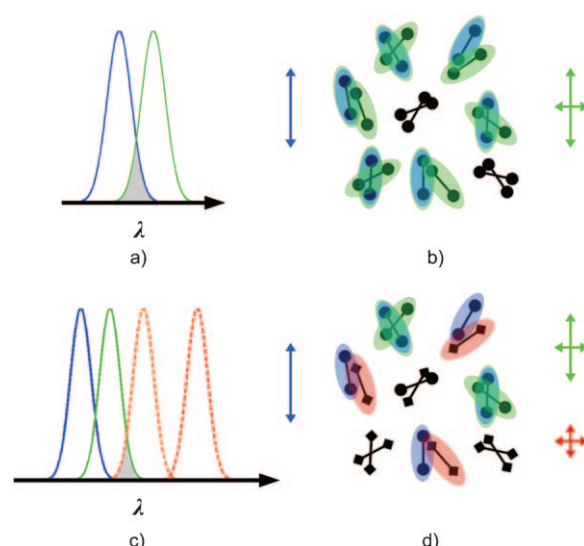
Figure 1. Fluorescence anisotropy spectroscopy and microscopy. Fluorescence-labelled molecules a) in a cuvette or b) on a microscope slide are excited with linearly polarised light (I_{ex}). The amount of depolarisation that has occurred during the lifetime of the fluorophore is measured by resolving the fluorescence intensity parallel and perpendicular to the excitation polarisation ($I_{\parallel}$ and $I_{\perp}$). Images of $I_{\parallel}$ and $I_{\perp}$ offer pixel-by-pixel anisotropy measurements, enabling intracellular features to be resolved.

Figure 2. Principles of HomoFRET and HeteroFRET. a) HomoFRET results from overlap between the absorption (blue) and emission (green) spectra of a single type of fluorophore. b) When homoFRET occurs in dimers, the emitted fluorescence consists of direct donor emission and sensitised acceptor emission. The fluorescence is thus not completely depolarised. c) Hetero-FRET results from overlap between the emission spectrum of one fluorophore (the donor ●, spectra in solid lines) and the absorption spectrum of a different fluorophore (the acceptor ◆, spectra in dotted lines). d) For hetero-FRET, two types of fluorophores are present (● and ◆), and fluorophores ● are selectively excited with polarized light at its absorption wavelength (blue). Only a proportion of the population consists of both types of fluorophores that give rise to a heteroFRET signal. The fluorescence due to hetero-FRET (red) can be spectrally separated from the homoFRET signal (green) and is more depolarised as heteroFRET is irreversible . The area highlighted in grey represents the spectral overlap where FRET occurs. Molecules whose dipoles are not aligned with the polarisation of the excitation light are not excited (Section 2.2). In (b) and (d), the blue arrows represent the excitation light; the green and red arrows represent the emitted fluorescence from ● and ◆ respectively. The length of the vertical and horizontal arrows represent the magnitude of $I_{\parallel}$ and $I_{\perp}$ respectively.

where $I_{\parallel}$ and $I_{\perp}$ are the fluorescence intensity in the polarisation orientations parallel and perpendicular to that of the excitation light, and G is the calibration factor that accounts for the different detection sensitivities for light of the different polarisations. The determination of G is crucial for successful FAIM imaging and is discussed in Section 5.

Figure 1 illustrates the essentials of a) spectroscopic measurements in cuvettes and b) FAIM. Linearly polarised light is used to selectively excite fluorophores with dipoles in similar orientations (this process is known as photoselection). The degree of depolarisation that occurs during the lifetime of the excited fluorophore is measured by resolving $I_{\parallel}$ and $I_{\perp}$ relative to the polarisation of the excitation light. Fluorescence depolarisation occurs mainly due to rotational diffusion and FRET between molecules of different orientations. Therefore, FAIM can provide spatially resolved information on rotational mobility, molecular binding, or clustering of fluorescently labelled molecules.[23–25]

As an example, the effects of homoFRET and heteroFRET on the emitted fluorescence from dimers labelled with one or two types of fluorophores are illustrated in Figure 2. In homoFRET, only one type of fluorophore is present. When fluorophores are randomly oriented in dimers, the fluorescence emission becomes depolarised relative to the linearly polarized excitation light when homoFRET occurs. Because the same fluorophore moiety acts both as the donor and acceptor in homoFRET, energy transfer is reversible. This transfer of energy back to the original donor, in addition to direct donor emission, give rise to donor emission with a polarisation which is preferentially orientated along the polarisation direction of the original excitation light. As a result, the fluorescence emission when homo-FRET occurs contains contributions from acceptors as well as

donors and hence is not completely depolarised. On the other hand, the presence of two types of fluorophores (say A and B) in a heteroFRET experiment gives rise to a mixture of AA, AB and BB dimers. When the excitation light is tuned to the absorption peak of fluorophore A, the fluorescence consists of contributions from A (the homoFRET signal) and B (the hetero-FRET signal). In this case, the homoFRET and heteroFRET signals may be spectrally separated and thus the heteroFRET signal is more depolarised than the homoFRET signal.

HomoFRET depolarisation increases with the number of participating fluorophores. This effect presents an opportunity for cluster size quantification by measuring the degree of depolarisation. The maximum amount of homoFRET depolarisation for a defined cluster occurs when the energy transfer has reached equilibrium, that is, a point where all molecules in the cluster have an equal probability of emitting a photon. Thus, the larger the number of molecules in a cluster, the lower the anisotropy of the overall fluorescence is due to increasing contributions from sensitised acceptor emission. This is illustrated in Figures 4 b,c. Runnels and Scarlata[26] derived a set of equations to predict the amount of depolarisation based on cluster size
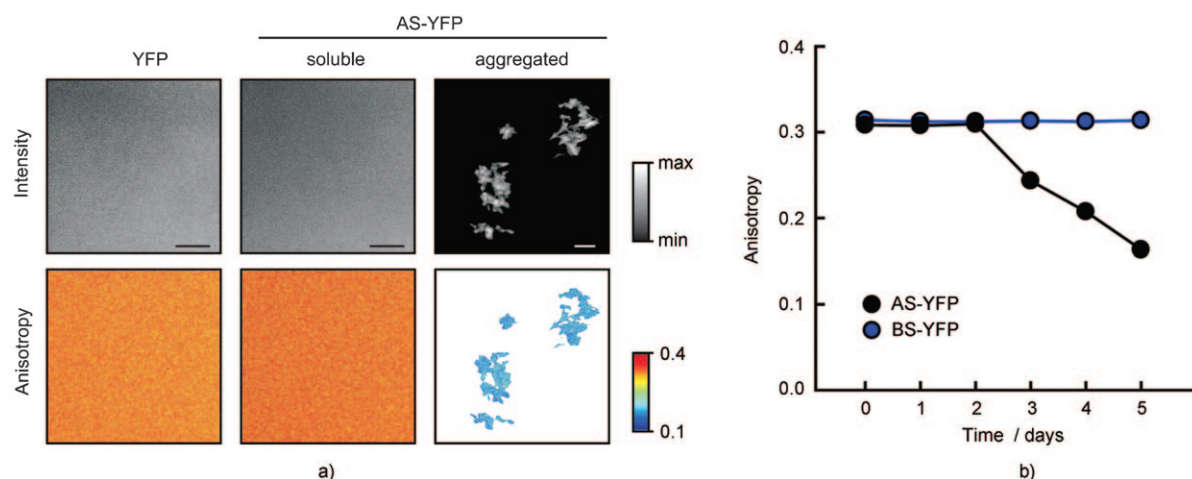
Figure 3. FAIM images of YFP-labelled alpha-synuclein aggregates in vitro. HomoFRET among YFP-labels on aggregated recombinant alpha-synuclein (AS) leads to depolarised fluorescence. a) Fluorescence intensity (top row) and anistropy (bottom row) images of AS-YFP in soluble and aggregated form (columns 2 and 3). Column 1 shows a control experiment for purified YFP in solution. b) Spectroscopic measurements of anisotropy show a decrease in the spatially averaged anisotropy as a function of aggregation time. For beta-synuclein (BS), which does not aggregate, no change in *r* is observed.[27] Reprinted from T. J. van Ham, A. Esposito, J. R. Kumita, S.-T. D. Hsu, G. S. Kaminski Schierle, C. F. Kaminski, C. M. Dobson, E. A. A. Nollen, C. W. Bertoncini, *J. Molec. Biol.* **2010**, *395*, 627–642, with permission from Elsevier.

(up to four) and interfluorophore distance within the cluster. It should be noted that the incremental decrease in overall anisotropy becomes smaller as cluster size increases, making the technique more useful for quantifying smaller clusters. This, however, does not preclude the usefulness of homoFRET to detect the presence of larger clusters. For example, in ref. [27] homoFRET anisotropy imaging was used to study large amyloid aggregates of alpha-synuclein in vitro as a model of Parkinson's disease (Figure 3). The example shows that upon aggregation, the high anisotropy for soluble monomeric proteins decreases due to homoFRET among the attached YFP-labels. A decrease in anisotropy was also observed in solutions as a function of aggregation time (measured in a spectrofluorometer), whereas no change was observed for beta-synuclein, which does not aggregate (Figure 3b). The observed anisotropy changes cannot be uniquely related to changes in oligomer size, but indicate changes in the relative fraction of monomeric and aggregated species in the measurement volume. Such methods may be useful to screen for, and assess the efficacy of, anti-aggregating drugs. Some attempts at quantifying homoFRET from large clusters have been made. For example, the effect of homoFRET in large aggregates on the time-resolved anisotropy of the fluorescence has been predicted using Monte Carlo simulations, based on assumptions on the protein aggregate structure and fluorophore-labelling frequency.[28]

In addition to homoFRET, rotational diffusion of molecules also causes depolarisation of fluorescence emission. Molecules with a rotational correlation time Θ shorter than their fluorescence lifetime τ_D emit fluorescence, the polarisation vector of which is correspondingly rotated relative to the excitation field (illustrated in Figure 4a). For homoFRET studies, it is beneficial to have a system in which rotational depolarisation is negligible. This may be accomplished by using a fluorescent probe for which $\Theta \gg \tau_D$. Fortunately, most fluorescent proteins satisfy
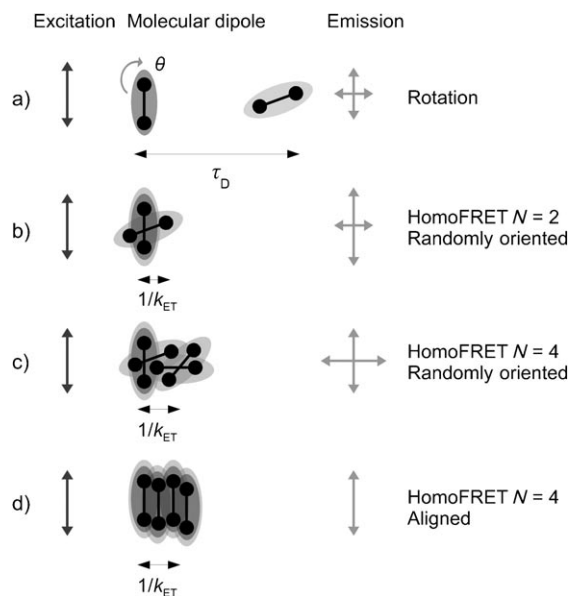
Figure 4. Depolarisation by rotational diffusion and homoFRET. Fluorophores excited by linearly polarised light emit depolarised fluorescence due to rotational diffusion and/or homoFRET. a) A fluorophore with rotational correlation time Θ shorter than its fluorescence lifetime τ_D emits fluorescence with polarisation orientation unaligned with that of the excitation light. b), c) HomoFRET between randomly-oriented fluorophores in clusters leads to depolarised emission—bigger clusters lead to more depolarised fluorescence emission. d) However, if molecular dipoles of the fluorophores in a cluster are aligned with each other, little depolarisation will occur. HomoFRET occurs on a shorter timescale than rotational diffusion ($t \approx 1/k_{ET}$ for FRET and Θ for rotational diffusion), allowing experimental identification by time-resolved anisotropy measurements (see Figure 5).

this criterion (e.g. $\tau_D \sim 3$ ns and $\Theta \sim 20$ ns for free GFP in aqueous solution, which represents the lower limit of Θ for GFP-labelled proteins[29]). Furthermore, techniques which vary homoFRET efficiency but not the rate of rotational diffusion, for ex-
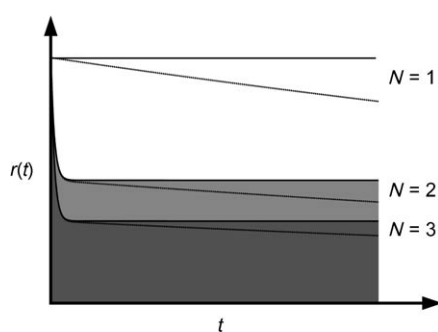
ample, through photobleaching, varying labelling frequency and red-edge excitation of fluorophores,[30,31] can be used to distinguish the homoFRET depolarisation component from that caused by rotational diffusion.

3. HomoFRET Fluorescence Anisotropy Imaging: Practical Details

3.1. Instrumentation

The simplest implementation of FAIM is achieved by addition of polarisers in the excitation and emission paths of the microscope system. Two consecutive images are recorded and the emission polariser is rotated from a parallel to a perpendicular orientation relative to the excitation polariser between recordings. However, for biological experiments simultaneous detection is favoured as samples tend to drift and/or photobleach. Here, a polarising beam-splitter is often used in the emission path, directing fluorescence of each polarisation to a separate detector. Another method for simultaneous detection makes use of a Wollaston crystal which separates the polarisations in the emission spatially for their subsequent detection on different areas of a detector array. This allows faster detection and provides potential for incorporating multidimensional fluorescence measurements, for example, a combination of simultaneous spectral and anisotropy detection.[32]

Like all fluorescence methods, FAIM can be carried out in steady-state or time-resolved mode. Figure 5 illustrates how steady-state and time-resolved anisotropy measurements can be used to identify rotational and homoFRET depolarisation. As homoFRET occurs on a much faster timescale than rotation diffusion for GFP in live cells,[33,29] a measurement of the time-resolved anisotropy decay permits the two to be separated by resolving the multi-exponential decay components. Steady-state experiments are much simpler to implement, but data

are temporally averaged [equivalent to the area under the plot of $r(t)$ as a function of time, see Figure 5]. As a result, the information on homoFRET contained in the rate of the anisotropy decay is lost. On the other hand, setup and data analysis for time-resolved techniques are much more complex and only a few studies on time-resolved FAIM have been reported so far.[33–36] One requires a pulsed excitation source and time-correlated detection of $I_\parallel(t)$ and $I_\perp(t)$ by fluorescence lifetime imaging (FLIM) to measure the time-resolved anisotropy $r(t)$, which is defined by Equation (4):

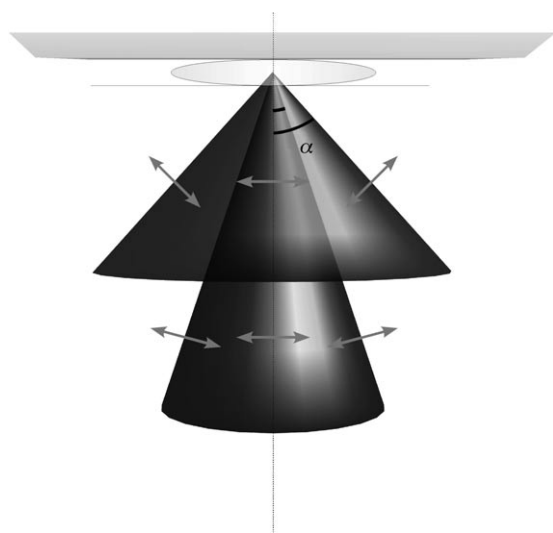$$r(t) = \frac{I_\parallel(t) - GI_\perp(t)}{I_\parallel(t) + 2GI_\perp(t)} \tag{4}$$

where $I_\parallel(t)$ and $I_\perp(t)$ are intensity decay functions of the parallel and perpendicular emissions deconvolved from the respective instrument response functions.[25] For the study of self-assembly, the additional information contained in the time-resolved measurement of anisotropy decay $r(t)$ can provide further insights into the system, such as cluster sizes and distributions.[37,33] Figure 5 illustrates how homoFRET, cluster size and rotation affect $r(t)$.

3.2. FAIM Implementation Guidelines

The quantification of fluorescence anisotropy using a microscope setup presents specific challenges. Subtle variations in the experimental conditions can cause large uncertainties in the measurement. In the following section a few of the most important experimental issues are summarised to encourage a rigorous approach.

3.2.1. Microscope Optics

FAIM of molecular clusters relies on the accurate measurement of the degree of depolarisation between the excitation light and emitted fluorescence, caused by homoFRET. However, the multitude of optical components in a microscope inevitably also leads to depolarisation of light, which introduces systematic error to the anisotropy measurement. In particular, the microscope objective causes a mixing of different polarisation components because excitation and emission light cones subtend large solid angles α from the sampling point (Figure 6).[38] For objectives with large numerical apertures, where $NA = \sin\alpha$, the measured anisotropy r will be lower than the theoretical value (or that measured on a spectrofluorometer). The discrepancy depends not only on the specific combination of optical components in a microscope system, but also on the position of a pixel in the field of view. Hence, there is no general algorithm to correct for this. One can measure the degree of depolarisation caused by microscope optics by comparing measurements of r for a fluorescent dye of small hydrodynamic radius in solvents of varying viscosity against those from a commercial spectrofluorometer. For example rhodamine 6G can be used in water with increasing proportions of glycerol. The problem can be ameliorated (but not avoided altogether) by

Figure 5. Time-resolved anisotropy decay $r(t)$ resulting from depolarisation from rotational diffusion and homoFRET. HomoFRET occurs on a shorter timescale than rotational diffusion, and its presence can be detected as a fast decay component in the time-resolved anisotropy decay. The solid lines denote typical anisotropy decays for N fluorophores in a cluster, with negligible rotational diffusion; the dotted lines are those with detectable rotational diffusion indicated by the presence of a slower decay component. Steady-state anisotropy measurements are temporally-averaged, and are denoted by the area under the curves. Larger clusters lead to both lower steady-state r and r_∞ (r at long times) values, but the incremental decrease in anisotropy reduces for increasing cluster size N.[26]

Figure 6. Depolarisation by microscope objectives. Light subtends a larger solid angle at the sample when focused by an objective with a high numerical aperture (NA), introducing more mixing of horizontal and vertical polarisations.[38]

avoiding the use of high NA objectives (>0.75)[39] or by measuring anisotropy changes relative to those from a control sample (e.g. a sample of solely monomers). The former inevitably leads to loss of spatial resolution.

One also requires a calibration to determine the G factor, which appears in Section 2.2 and accounts for the difference in sensitivity of the detection optics to light of different polarisations. G may be estimated from a reference with a known anisotropy value r_{ref} according to Equation (5) below. This is most easily obtained with a fast-rotating dye, for which $r_{ref} \approx 0$. It is important that a dye is chosen with an emission spectrum close to that of the sample to be measured, as G is wavelength-dependent:[23, 24, 39]

$$G = \frac{I_{\parallel}(1 - r_{ref})}{I_{\perp}(1 + 2r_{ref})} \qquad (5)$$

3.2.2. Fluorescence Intensity and Light Scattering

Determination of the fluorescence anisotropy r relies on precise intensity measurements. Great care must be taken not to saturate the fluorescence emission and to choose an excitation intensity range for which signals vary linearly. Saturation causes enhanced excitation of misaligned fluorophores (degradation of the photoselection process mentioned in Section 2.2), and results in an underestimation of the anisotropy value.[40] Secondly, photobleaching must be minimised as it reduces the number of fluorophores on the probed molecular clusters. Therefore, significant photobleaching increases the effective distance R between fluorophores and thus reduces the homoFRET efficiency. This effect leads to an underestimation of the cluster size.

On the other hand, the fidelity of anisotropy measurements increases with photon number,[40] and hence there is an opti-

mal balance between maximising available signal whilst keeping fluorophore saturation and photobleaching at acceptable levels. There are important consequences associated with the nature of imaging biological samples: in live cells, the expression levels of fluorescent proteins may fluctuate in time, and the sample environment and signal levels are continuously changing. Because of these temporal drifts in the sample as well as instrumental drifts, it may be difficult to compare anisotropy data obtained from sequential recordings. Errors arising in the comparison of data from separate images are usually higher than those from different locations within the same image, as drifts are less significant in the latter case.[41]

Light scattering in thick samples also leads to a depolarisation of excitation and fluorescence light.[42–44] Monte Carlo simulations and data from experiments presented in refs. [43, 44] have shown that anisotropy values decrease with increasing number of scattering events. This effect can be pronounced when imaging turbid biological samples and can be partially suppressed through the use of low NA objectives and appropriately selected pinholes in confocal microscopy. These measures help in the rejection of scattered light and thus in the preservation of the polarisation state, but also lead to loss of resolution and a reduction in the signal-to-noise ratio with the associated problems discussed in Section 3.2.2.

3.2.3. Image Post-Processing

Computation of r in every image pixel requires quantitative image processing from images corresponding to $I_{\parallel}$ and $I_{\perp}$ signals [according to Eq. (3)], which are subject to Poisson noise. In addition, the factors discussed in the preceding sections can cause large standard deviations in the measured r within and between images, even for identical cluster sizes, which can hinder meaningful interpretation of the underlying molecular states. Post-processing can improve signal-to-noise ratios and therefore anisotropy resolution. Spatial filtering such as Gaussian or median filtering have been applied to background-corrected $I_{\parallel}$ and $I_{\perp}$ images before computation of r images.[40] Sensibly applied, such filters can improve the overall quality of the obtained anisotropy images.

4. Case Studies

4.1. Detecting Cellular Membrane Rafts

The organisation of proteins and lipids into domains in cellular membranes ("membrane rafts") has been considered to be an essential feature of their function, but the detection of such domains in membranes of living cells has not been straightforward. The main challenges are posed by the phase of the membrane as an ordered liquid, and the small size (100–200 nm) and dynamic nature of the hypothesised rafts.[45] Varma and Mayor[30] applied homoFRET anisotropy imaging to detect domains for glycosylphosphatidylinositol (GPI)-anchored proteins in membranes of live cells, providing compelling evidence for their existence. The design of the experiment was based on a hypothesis that the homoFRET efficiency should

vary differently with fluorophore density, depending on whether the proteins are randomly distributed across the membrane (i.e. absence of membrane rafts) or clustered into domains (i.e. presence of membrane rafts). The homoFRET induced depolarisation should increase with density in randomly distributed proteins, whereas no such dependence on density would be expected for domain-bound proteins. The experiments revealed uniform anisotropy distributions in labelled GPI-anchored protein expressing cells. By photobleaching and thus reducing the fluorophore density, an increase in the anisotropy was observed in cells expressing GPI-anchored proteins, consistent with the lipid raft hypothesis. In contrast, little change was observed on photobleaching cells expressing randomly distributed transmembrane-anchored proteins.

The methodology was extended in a number of ways by Sharma et al.[46] Firstly, it was applied to demonstrate the existence of clusters of various GPI-anchored proteins in multiple cell lines. Secondly, time-resolved anisotropy measurement by sequential $I_\parallel(t)$ and $I_\perp(t)$ measurements, using FLIM with TCPSC, was used to identify homoFRET depolarisation. An estimate of the inter-fluorophore distance R of < 4 nm was derived from the homoFRET rate, determined by the fast anisotropy decay component, using Förster's equations. It is worth noting that this analysis involves the fitting of a two-component exponential decay to the time-resolved anisotropy, which is only approximate for clusters of $N > 2$. Thus, the ability of this approach to quantify cluster size accurately using homoFRET is limited, although complementary control experiments described in that paper[46] suggest indeed that the domains are small and consist of only a few molecules. Moreover, they derived a model to predict the anisotropy change with decreasing fluorophore concentrations based on how the GPI-anchored proteins could be organised on the cell surface: 1) proteins are all in domains, 2) protein domains coexist with isolated proteins distributed on the surface and 3) proteins are arranged uniformly along the periphery of individual domains. It was found that experimental data were consistent with model 2. Based on anisotropy measurements, Sharma et al.[46] were then able to determine the co-localisation of multiple GPI-anchored proteins in the same cluster and the influence of cholesterol and cross-linking on these clusters, thus giving more insights into their biological function.

These studies demonstrate the value of homoFRET anisotropy imaging in helping to elucidate biological problems that are especially challenging for traditional biophysical or biochemical assays. The work is a particularly good example of the level of detail and biological insight that can be obtained through the combined application of advanced imaging, and sound qualitative and quantitative reasoning in a hypothesis driven approach to the problem. Other fluorescence methods of studying lipid rafts in live cells have also been developed.[47–49] For example, the fluorescent probe laurdan has an emission spectrum that is sensitive to the water content in membranes, and a comparison of fluorsecence intensities emitted in the regions 400–460 nm and 470–530 nm informs on the ordering of lipids in membrane rafts.[47,48] Stimulated emission depletion (STED) microscopy with fluorescence correlation spectroscopy (FCS) has also been used to show that species hypothesised to be in rafts exhibit restricted diffusion in domains of $< \sim 20$ nm in diameter, revealing heterogeneity in their distribution on the plasma membrane.[49] The application of STED improves spatial resolution in the *x–y* plane to below the wavelength of light, and, when combined with FCS, is particularly suited to detecting small and transient entities. Although both methods can be operated to be compatible with studies in live cells, they provide limited information on the molecular organisation in the rafts but are useful complements to homoFRET.

4.2. Detecting and Sizing Protein Clusters

HomoFRET anisotropy has been widely applied in spectroscopic studies to detect oligomerisation of proteins. Far fewer have been extended to imaging. Gautier et al.[35] utilised fluorescence steady-state and time-resolved anisotropy measurements to demonstrate the ability of homoFRET detection by identifying a fast component in the anisotropy decay. Based on the known dimeric structure of the crystallised protein from X-ray diffraction and a symmetric dimer model, the homoFRET rate and the relative orientation between the two GFP chromophores were estimated from the measured anisotropy decay. Lidke et al.[50] utilised a technique called rFLIM[51] based on frequency-domain lifetime imaging for this purpose. Again the authors observed an increase in anisotropy of a GFP-labelled cell-surface protein in cells upon photobleaching and a concomitant reduction in labelling frequency, interpreted as evidence for homoFRET due to the formation of homo-dimers or -oligomers. Marquer et al.[52] also applied steady-state anisotropy imaging to detect the homo-dimerisation of a G-protein-coupled receptor in live cells by measuring a decrease in anisotropy due to homoFRET when cells are incubated with a ligand that stabilises the homodimeric form of the receptor.

Earlier homoFRET studies for protein self-assembly as described above focused mainly on detecting reduced anisotropy upon cluster formation and attributing the effect to homoFRET. Bader et al.[33,53] report on a promising development of the technique to enable the quantification of protein cluster sizes. The technique, named cluster size imaging, is based on measuring time-resolved anisotropy in the extreme tail of the signal decay. The measured residual anisotropy, r_∞, requires only a moderate temporal resolution in the time-resolved anisotropy measurement (only four time gates with ns resolution in refs. [33,53]) and hence simpler instrumentation. Theoretical arguments reported in refs. [26,37] show that homoFRET in clusters leads to an r_∞ which may be expressed as a function of r_0 for monomers and N, the cluster size, under the assumptions that: 1) the orientations of the fluorophores are random (Figure 4), 2) the depolarisation due to rotational diffusion is negligible (Figure 5) and 3) the homoFRET rate is much faster than the rate of fluorescence. Under these assumptions, a measurement of r_0 and r_∞ yields an estimate of the protein cluster size N. Assumption (3) implies that energy exchange by homoFRET has reached equilibrium in the cluster and the probability of photon emission is equal for all fluorophores in the cluster

when r_{∞} is recorded. As demonstrated in ref. [33], this is usually valid for small clusters for which the homoFRET efficiency is greater than 0.5.
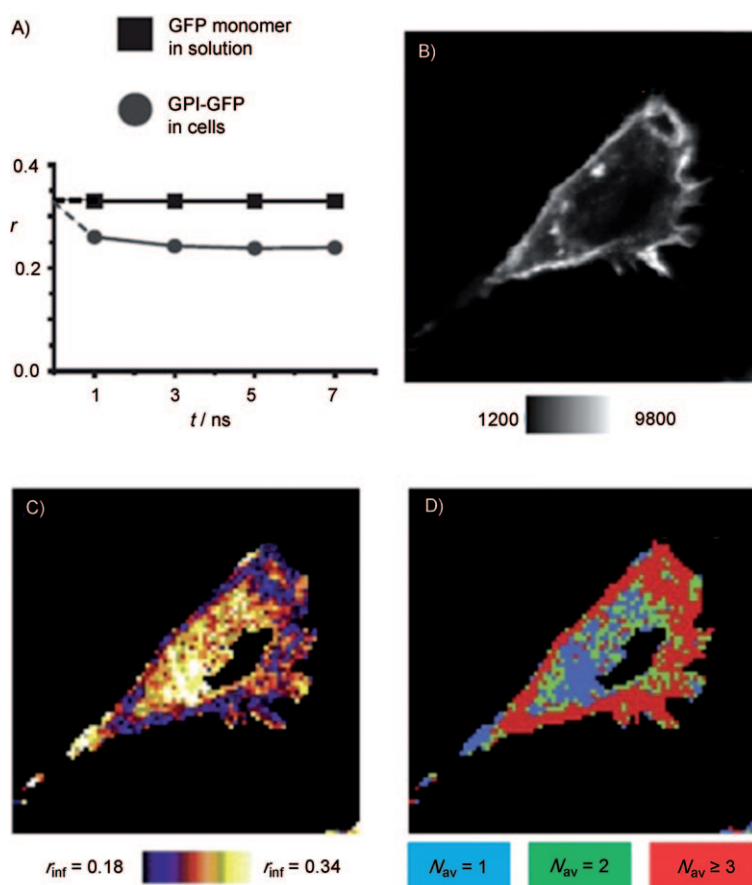
The analysis becomes more complex if the fluorophores are partially aligned (as may happen for membrane proteins for example, or other highly ordered oligomeric structures).[53] In this case, the orientation of the acceptor fluorophore is correlated to that of the donor fluorophore, reducing the degree of depolarisation due to homoFRET and limiting the applicability of the theory by Runnels and Scalata (Figure 4).[26] To circumvent this problem, Bader et al.[53] created constructs for controlled oligomerisation of GFP in the cytoplasm and nucleus of cells, and measured values of r_{∞}/r_0 for dimers and higher oligomers as references for calibration. Under the assumption that the cytosolic contructs can be used as controls for membrane protein systems, the anisotropy images based on r_{∞} of the system can be converted to cluster size images using the obtained calibration values. Figure 7 shows the intensity, r_{∞} and cluster size images of a live cell, revealing the clustering propensity of GPI-anchored proteins in the plasma membrane. The advantage of measuring cluster sizes based on r_{∞} is that relatively simpler instrumentation with low time resolution is

required because the complete anisotropy decay need not be resolved. However, the study also highlights two major limitations in the use of homoFRET to quantify protein cluster sizes in cells. Firstly, existing models relating anisotropy to cluster size all rely on the assumption that the dipoles of the fluorophores are randomly oriented, because FAIM is inherently unable to detect clusters in which the dipoles are perfectly aligned (Figure 4). Secondly, as noted by Bader et al., the reported cluster sizes represent average values of all clusters in the detection volume, which is typically $> \sim 0.01\ \mu m^3$ and contains many molecules. Hence, the average cluster size as inferred from FAIM data must be treated with caution because there may not be a unique relationship between spatially averaged FAIM data and the distribution of cluster sizes in the sample volume. An alternative method for sizing protein clusters has been presented by Yeow and Clayton,[54] who developed an analytical method for deducing size distribution of oligomers by theory relating the steady-state anisotropy and labelling frequency, an approach similar to that of Sharma et al.[46] Their model, based on the binomial distribution of clusters of different labelled fractions and a linear combination of anisotropy from each fraction, predicts that the steady-state anisotropy as a function of labelling frequency of a cluster of size N is a polynomial of order $N-1$. This method is theoretically capable of determining minimum cluster sizes when the sample contains mixtures of monomers and clusters, as the effect of reducing the labelling fraction increases the anisotropy from clusters but leaves the anisotropy of monomers unchanged. However, in the analysis for cluster size quantification it is subsequently assumed that the anisotropy of clusters containing more than one fluorophore is zero, which is not generally valid because of direct donor emission and the reversibility of homoFRET (Section 2.2).

Figure 7. Protein cluster size imaging in cells. A) Time-resolved anisotropy measurements by time-gated detection at 1, 3, 5 and 7 ns reveal homoFRET in GPI–GFP in cells. B) is an intensity-only image. C) Pixel-by-pixel measurement of r_{∞} values is converted to a cluster size image (D), showing average cluster size $N_{av} \geq 3$ in the plasma membrane.[53] Reprinted from A. N. Bader, E. G. Hofman, J. Voortman, P. M. P. van Bergen en Henegouwen, H. C. Gerritsen, *Biophys. J.* **2009**, *97*, 2613–2622, with permission from Elsevier.

5. Summary

Over the last decade or so there have been significant advances in the development of quantitative methods for the determination of homoFRET in a microscope setting, opening yet another avenue along which Förster's work will continue to generate scientific momentum. This article reviews theory and application of homoFRET with a particular focus on studies of molecular clustering in a biological environment. Whilst the method theoretically appears to be suited for this task, there are considerable practical challenges: depolarisation of excitation and fluorescence light through microscope optics and the heterogeneity of biological samples such as cells can cause large random and systematic errors and complicate the interpretation of measured data. These also make accurate quantification of cluster sizes difficult. As a result there are still only a handful of reported homoFRET microscopy experiments that have produced genuine insight in the field of molecular

clustering in the life sciences. However there are signs that this situation is about to change. Considerable efforts have been made to quantify effects of microscopic optics on the measured anisotropy values and to improve the spatial resolution obtainable in homoFRET measurements.[40,44] The effects of fluorophore clustering on fluorescence depolarisation due to homoFRET have been studied theoretically,[26,28,46,54] permitting in-depth analyses of acquired homoFRET data. These developments have set a sound basis for future ventures to apply homoFRET anisotropy imaging to unsolved problems in the life sciences.

6. Outlook

Ongoing developments to improve anisotropy resolution in the cellular environment and to combine anisotropy imaging with multiparametric or super-resolution fluorescence imaging techniques will enable researchers to gain more insights into the self-assembly process and relate it to cellular functions.[32,55–58] There is also potential for using anisotropy imaging for unsupervised imaging modalities and high-throughput screening.[59] So far the sizing of clusters has been limited to relatively small clusters (< 4 molecules) because the sensitivity of current methodologies diminishes rapidly with cluster size. An extension to permit characterisation of clusters of larger size would considerably widen the applicability of the technique. An application field of huge biomedical importance that would benefit from such developments relates to protein aggregation in neurodegenerative disease. HomoFRET anisotropy imaging has very recently been applied in the study of amyloid formation in models of Parkinson's and related diseases in vitro.[27] A capability to detect and size early cytotoxic oligomers and protofibrils (made up of ~ 2–20 molecules) of these amyloidogenic proteins in live cells would generate great impact in the understanding of these highly debilitating diseases.[3,60,61]

[1] L. J. Pike, *J. Lipid Res.* **2006**, *47*, 1597.
[2] M. Vendruscolo, J. Zurdo, C. E. MacPhee, C. M. Dobson, *Philos. Trans. R. Soc. A* **2003**, *361*, 1205.
[3] F. Chiti, C. M. Dobson, *Annu. Rev. Biochem.* **2006**, *75*, 333.
[4] T. S. Burkoth, T. L. S. Benzinger, V. Urban, D. M. Morgan, D. M. Gregory, P. Thiyagarajan, R. E. Botto, S. C. Meredith, D. G. Lynn, *J. Am. Chem. Soc.* **2000**, *122*, 7883.
[5] D. G. Lynn, S. C. Meredith, *J. Struct. Biol.* **2000**, *130*, 153.
[6] Y. L. Lyubchenko, B. H. Kim, A. V. Krasnoslobodtsev, J. Yu, *Wiley Interdiscip. Rev. Nanomed. Nanobiotechnol.* **2010**, *2*, 526.
[7] D. J. Stephens, V. J. Allan, *Science* **2003**, *300*, 82.
[8] X. W. Dai, Z. L. Yue, M. E. Eccleston, J. Swartling, N. K. H. Slater, C. F. Kaminski, *Nanomed. Nanotechnol.* **2008**, *4*, 49.
[9] A. Esposito, S. Schlachter, G. S. K. Schierle, A. D. Elder, A. Diaspro, F. S. Wouters, C. F. Kaminski, A. I. Iliev, *Methods Mol. Biol.* **2009**, *586*, 117.
[10] S. Inouye, F. I. Tsuji, *FEBS Lett.* **1994**, *341*, 277.
[11] G. Patterson, *Biophys. J.* **1997**, *73*, 2782.
[12] R. Y. Tsien, *Annu. Rev. Biochem.* **1998**, *67*, 509.
[13] M. J. Roberti, C. W. Bertoncini, R. Klement, E. A. Jares-Erijman, T. M. Jovin, *Nat. Methods* **2007**, *4*, 345.
[14] C. Kaminski, *J. R. Soc. Interface* **2009**, *6*, S1.
[15] Y. Yan, *Curr. Opin. Chem. Biol.* **2003**, *7*, 635.
[16] J. Eisinger, *Q. Rev. Biophys.* **1976**, *9*, 21.
[17] M. Rao, S. Mayor, *Biochim. Biophys. Acta Mol. Cell Res.* **2005**, *1746*, 221.
[18] T. Förster, *Naturwissenschaften* **1946**, *33*, 166.
[19] F. Perrin, *Ann. Phys.* **1929**, *12*, 169.
[20] E. A. Jares-Erijman, T. M. Jovin, *Nat. Biotechnol.* **2003**, *21*, 1387.
[21] D. W. Piston, G. J. Kremers, *Trends Biochem. Sci.* **2007**, *32*, 407.
[22] A. D. Elder, A. Domin, G. S. Kaminski Schierle, C. Lindon, J. Pines, A. Esposito, C. F. Kaminski, *J. R. Soc. Interface* **2009**, *6*, S59. 12.
[23] J. Dix, *Biophys. J.* **1990**, *57*, 231.
[24] A. H. Gough, D. L. Taylor, *J. Cell Biol.* **1993**, *121*, 1095.
[25] M. Tramier, T. Piolot, I. Gautier, V. Mignotte, J. Coppey, K. Kemnitz, C. Durieux, M. Coppey-Moisan, *Methods Enzymol.* **2003**, *360*, 580.
[26] L. W. Runnels, S. F. Scarlata, *Biophys. J.* **1995**, *69*, 1569.
[27] T. J. van Ham, A. Esposito, J. R. Kumita, S. T. D. Hsu, G. S. Kaminski Schierle, C. F. Kaminski, C. M. Dobson, E. A. A. Nollen, C. W. Bertoncini, *J. Mol. Biol.* **2010**, *395*, 627.
[28] D. Marushchak, L. B. A. Johansson, *J. Fluoresc.* **2005**, *15*, 797.
[29] R. Swaminathan, C. P. Hoang, A. S. Verkman, *Biophys. J.* **1997**, *72*, 1900.
[30] R. Varma, S. Mayor, *Nature* **1998**, *394*, 798.
[31] A. Squire, P. J. Verveer, O. Rocks, P. I. H. Bastiaens, *J. Struct. Biol.* **2004**, *147*, 62.
[32] G. Harms, *Biophys. J.* **1999**, *77*, 2864.
[33] A. N. Bader, E. G. Hofman, P. M. P. van Bergen en Henegouwen, H. C. Gerritsen, *Opt. Express* **2007**, *15*, 6934.
[34] A. J. Cross, G. R. Fleming, *Biophys. J.* **1984**, *46*, 45.
[35] I. Gautier, *Biophys. J.* **2001**, *80*, 3000.
[36] J. Siegel, K. Suhling, P. M. P. Lanigan, S. E. D. Webb, D. Phillips, D. M. Davis, P. M. W. French, *Rev. Sci. Instrum.* **2003**, *74*, 182.
[37] F. Tanaka, N. Mataga, *Photochem. Photobiol.* **1979**, *29*, 1091.
[38] D. Axelrod, *Biophys. J.* **1979**, *26*, 557.
[39] C. E. Bigelow, D. L. Conover, T. H. Foster, *Opt. Lett.* **2003**, *28*, 695.
[40] K. A. Lidke, B. Rieger, D. S. Lidke, T. M. Jovin, *IEEE T Image Process* **2005**, *14*, 1237.
[41] Q. S. Hanley, V. Subramaniam, D. J. Arndt-Jovin, T. M. Jovin, *Cytometry A* **2001**, *43*, 248.
[42] F. W. J. Teale, *Photochem. Photobiol.* **1969**, *10*, 363.
[43] J. M. Schmitt, A. Knuttel, M. Yadlowsky, *J. Opt. Soc. Am. A* **1994**, *11*, 2226.
[44] C. E. Bigelow, T. H. Foster, *J. Opt. Soc. Am. A* **2006**, *23*, 2932.
[45] K. Jacobson, O. G. Mouritsen, R. G. W. Anderson, *Nat. Cell Biol.* **2007**, *9*, 7.
[46] P. Sharma, R. Varma, R. C. Sarasij, Ira, K. Gousset, G. Krishnamoorthy, M. Rao, S. Mayor, *Cell* **2004**, *116*, 577.
[47] F. M. Harris, K. B. Best, J. D. Bell, *Biochim. Biophys. Acta Biomembr.* **2002**, *1565*, 123.
[48] K. Gaus, E. Gratton, E. P. W. Kable, A. S. Jones, I. Gelissen, L. Kritharides, W. Jessup, *Proc. Natl. Acad. Sci. USA* **2003**, *100*, 15554.
[49] C. Eggeling, C. Ringemann, R. Medda, G. Schwarzmann, K. Sandho, S. Polyakova, V. N. Belov, B. Hein, C. von Middendor, A. Schonle, S. W. Hell, *Nature* **2009**, *457*, 1159.
[50] D. S. Lidke, P. Nagy, B. G. Barisas, R. Heintzmann, J. N. Post, K. A. Lidke, A. H. A. Clayton, D. J. Arndt-Jovin, T. M. Jovin, *Biochem. Soc. Trans.* **2003**, *31*, 1020.
[51] A. Clayton, Q. Hanley, D. Arndt-Jovin, V. Subramaniam, T. Jovin, *Biophys. J.* **2002**, *83*, 1631.
[52] C. Marquer, C. Fruchart-Gaillard, G. Mourier, O. Grandjean, E. Girard, M. le Maire, S. Brown, D. Servent, *Biol. Cell* **2010**, *102*, 409.

[53] A. N. Bader, E. G. Hofman, J. Voortman, P. M. P. van Bergen En Henegouwen, H. C. Gerritsen, *Biophys. J.* **2009**, *97*, 2613.

[54] E. K. L. Yeow, A. H. A. Clayton, *Biophys. J.* **2007**, *92*, 3098.

[55] J. H. Frank, A. D. Elder, J. Swartling, A. R. Venkitaraman, A. D. Jeyasekharan, C. F. Kaminski, *J. Microsc.* **2007**, *227*, 203.

[56] I. Testa, A. Schonle, C. von Middendor, C. Geisler, R. Medda, C. A. Wurm, A. C. Stiel, S. Jakobs, M. Bossi, C. Eggeling, S. W. Hell, A. Egner, *Opt. Express* **2008**, *16*, 21093.

[57] S. Schlachter, S. Schwedler, A. Esposito, G. S. Kaminski Schierle, G. D. Moggridge, C. F. Kaminski, *Opt. Express* **2009**, *17*, 22747.

[58] S. Weidtkamp-Peters, S. Felekyan, A. Bleckmann, R. Simon, W. Becker, R. Kuhnemuth, C. A. M. Seidel, *Photochem. Photobiol. Sci.* **2009**, *8*, 470.

[59] D. R. Matthews, L. M. Carlin, E. Ofo, P. R. Barber, B. Vojnovic, M. Irving, T. Ng, S. M. Ameer-Beg, *J. Microsc.* **2010**, *237*, 51.

[60] S. Lesné, M. T. Koh, L. Kotilinek, R. Kayed, C. G. Glabe, A. Yang, M. Gallagher, K. H. Ashe, *Nature* **2006**, *440*, 352.

[61] G. M. Shankar, S. M. Li, T. H. Mehta, A. Garcia-Munoz, N. E. Shepardson, I. Smith, F. M. Brett, M. A. Farrell, M. J. Rowan, C. A. Lemere, C. M. Regan, D. M. Walsh, B. L. Sabatini, D. J. Selkoe, *Nat. Med.* **2008**, *14*, 837.